British Journal of Pharmacy

Research article

Searching for a long-acting injectable formulation for the antiretroviral dolutegravir

Marilene Alves[1]*, Anderson Aparecido de Marchi[1], Keity Margareth Doretto[2], Luis Gustavo Robello[2], Maiara Cássia Pigatto[2], Renar Santos Pereira[2], Claudia Bandeira Kobarg[2], Fabio Alessandro Proença Barros[2]

[1] Department of Pharmaceutical Research, EMS, Hortolândia, São Paulo, Brazil, [2] Vita Nova Institute, Hortolândia, São Paulo, Brazil.

ARTICLE INFO

ABSTRACT

The aim of this study was to engineer a proper particle size to provide plasma dolutegravir concentration maintenance above protein-adjusted 90% inhibitory concentration (PA-IC90) and to evaluate the monthly-acting injectable dolutegravir feasibility for HIV therapy. Liquid antisolvent precipitation technology was used to engineer dolutegravir particles. As a strategy for controlling variations of the habit, particle size and polymorphs of dolutegravir, process intensification was performed using acetone, methanol and dimethyl sulfoxide as solvents and temperature range from 5ºC to 30ºC. Physical properties of particles were characterized and *in vitro* drug release was measured. Results revealed that crystal morphology and polymorphic form were independents of solvent and temperature. Concerning solvents, particle sizes were not markedly different. However, results suggested that the higher temperature the higher dolutegravir particle size. Particle size, ranging from 6.48 µm to 17 µm, showed the maximum drug release of 93% in 12 days compared with raw drug that showed a maximum release of only 47.5%. *In vivo* pharmacokinetic analysis, conducted in Wistar male rats, demonstrated that dolutegravir particles of approximately 13 µm maintained plasma drug concentration above protein-adjusted 90% inhibitory concentration for 26 days.

INTRODUCTION

Dolutegravir free acid chemically known as (4R,12aS)-N-(2,4-difluorobenzyl)-7-hydroxy-4-methyl 6,8-dioxo-3,4,6,8,12,12a-hexahydro-2H-pyrido [1',2':4',5] pyrazino [2,1-b][1,3] oxazine-9 carboxamide, Figure 1, is a selective human immunodeficiency virus' (HIV) integrase enzyme inhibitor. Dolutegravir (DTG) works by inhibiting activity of the integrase enzyme, thereby preventing the viral deoxyribonucleic acid (DNA) from being integrated into the host cell's genetic material and blocking this stage of HIV replication (Cottrell *et al*; 2013).

This second-generation of integrase strand transfer inhibitors (INSTIs) combines the advantages of its predecessors such as raltegravir and elvitegravir, but it is administered once a day without the need for a pharmacokinetic booster and may be coformulated with other antiretrovirals in a single-tablet regimen (Osterholzer and Goldman, 2014). Additionally, DTG is rapidly absorbed, achieving maximal blood concentration 1.5–2.5 hours after oral ingestion and presents a terminal half-life of 12-15 hours (Cottrell *et al*; 2013). Because of its high potency, poor water-solubility and small oral dose, dolutegravir is a potential drug candidate for long-acting antiretroviral

therapy (LA-ART). Conceptually, LA-ART strategy relies on the idea that a highly potent and insoluble drug can be engineering into injectable medicines whose dose and volume are sufficient to achieve a sustained plasma drug exposure and reduced frequency of dosing. It is assumed that due to the very low solubility, drug particles as small as 200 nm dissolve slowly at the site of injection and allow sustained release over an extended period after injection (van´t Klooster et al; 2010; Trezza et al; 2015). Ultimately, such an approach would increase adherence of HIV patients to drug treatment once depending on drug properties, monthly or quarterly dosage could be achievable. In real, LA-ART has shown to be effective since promising clinical outcomes have been obtained with long-acting injectable formulation of rilpivirine (Baert *et al*; 2009) and cabotegravir (Trezza *et al*; 2015). Taking advantage of potency and water insolubility, injectable nanosuspensions based on rilpivirine and cabotegravir have progressed to a phase III trial named Antiretroviral Therapy as Long-Acting Suppression (ATLAS). Positive 48-week results showed that dual long-acting rilpivirine and cabotegravir, injected once a month and compared to a standard of care, daily, oral three-drug regimen, had similar efficacy in maintaining viral suppression in adults living with HIV-1 (Swindells *et al*; 2019).

In line with LA-ART approach, dolutegravir long-acting was simulated through physiologically-based pharmacokinetic (PBPK) modeling by Rajoli *et al* (2015). Primarily validated against oral clinical data using physicochemical properties, *in vitro* and population pharmacokinetic data, the PBPK model predicted a dolutegravir dose of 105 mg as a sufficient drug amount for monthly intramuscular administration. Naturally, a dolutegravir long acting injection would be possible if technological challenges to control its pharmacokinetics can be overcome. As a practical strategy, Silman *et al*., (2018) used high pressure homogenization to prepare an injectable suspension based on DTG particles on order of 368 nm. Preclinical results provided evidence that such formulation maintains drug concentrations above PA-IC90 for 14 days in treated mice. Once pharmacokinetic data were highly considered restrictive to dolutegravir long-acting success, Silman et al. (2018) modified dolutegravir molecule by attaching a myristoyl moiety to the drug structure. On this approach, the drug half-life and hydrophobicity of myristoyled-dolutegravir increased and consequently, nanosuspension based on 234nm-particles in size was formulated. Remarkably,

dolutegravir concentration remained over four times the protein-adjusted 90% inhibitory concentration (PA-IC90) for 28 days. Even though this new chemical entity presents a potential for future creation of long-acting injectable dolutegravir, as a prodrug, it presents a time-consuming and a more expensive regulatory pathway. Therefore, new approaches for long-acting formulation based on non-modified dolutegravir are very welcome once it would be an alternative approach to chemically-modified dolutegravir. Ultimately, the intention is always to maintain pharmacokinetic exposure constant and plasma concentrations within a targeted therapeutic window through a combination of drug potency, particles size and drug release rate. While rilpivirine (van´t Klooster et al; 2010) and cabotegravir (Trezza et al; 2015) long-acting were designed as nanoparticulate injectable suspension, apparently DTG cannot easily be transformed into long-acting medicines through such strategy once nanonization approach potentially increased drug release rate (Silman et al; 2018). On the other hand, the physical and chemical properties of DTG make it a good candidate for long-acting injectable (Cottrell et al; 2013). Therefore, such approach may be explored in microparticles domain. Naturally, the larger particle size may be highly restrictive to the requirements of injectable suspensions such as suspendability, injectability and patient comfort. In an ideal scenario, pharmaceutically acceptable suspensions should contain particle size less than 5 μm for subcutaneous and intramuscular administration (Jones, 2016; Owen and Rannard, 2016). However, conventional suspension-based injections have typically utilized larger particle size. For example, Depo-Medrol® (80 mg/ml - methylprednisolone acetate), and Celestone Soluspan® (6 mg/ml-betamethasone acetate) present particle size distribution across the 1- to 50 μm range with the greater particle percentage up to 20μm (Benzon et al; 2007). In this work, liquid antisolvent (LAS) precipitation is proposed as a technical approach for particle size control of dolutegravir. Basically, this technique involves the precipitation of a solid solute previously dissolved in an organic solvent by adding it into a non-solvent (antisolvent) under stirring (Meer et al; 2011). This well-established process provides a more convenient procedure at room temperatures and atmospheric pressure with no requirement of expensive equipment. Additionally, it is easily scalable as compared to other bottom-up methods. There are many papers available about the use of LAS for drug precipitation (Thorat and Dalvi, 2012). However, to the best of our knowledge, this paper is the first to use the LAS to precipitate dolutegravir free acid.
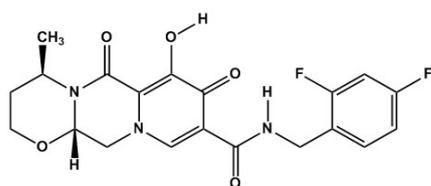
Fig 1: *Dolutegravir free acid structure (DTG)*

MATERIALS AND METHODS

Materials

Dolutegravir free acid (DTG), ((4*R*,12a*S*)-*N*-(2,4-difluorobenzyl)-7-hydroxy-4-methyl-6,8-dioxo-3,4,6,8,12,12a-hexahydro-2*H*-pyrido[1',2':4',5] pyrazino [2,1-b][1,3] oxazine-9 carboxamide), molecular weight 419.39 g/mol, was purchased from Laurus Private Limited (Visakhapatnam, India). Elvitegravir, ([[6-(3-chloro-2 fluorobenzyl)-1-[(2S)-1-hydroxy-3-methylbutan-2-yl]-] 7-methoxy-4-oxo-1, 4-dihydroquinolone-3 carboxylic acid]), molecular weight 447.89 g/mol, was purchased from Aurobindo Pharma Limited (Hyderabad, India). Poloxamer 338 (Kolliphor 338) was kindly provided by BASF Co., Ltd. (Brazil). Methanol, dimethyl sulfoxide (DMSO) and acetone were purchased from Sigma-Aldrich (Brazil). All reagents used in this study were reagent grade and used as received.

Methods
Raw DTG solubility in organic solvent

The solubility of DTG in acetone, methanol and DMSO was determined by successive dissolution of weighed portions of drug in a fixed volume of solvent at 25 °C. Solvent were recovered by filtration and evaporated. Solids were dried under vacuum and carefully weighted.

DTG particles precipitation by Liquid Antisolvent (LAS)

DTG was completely dissolved in 10 mL of solvent to reach drug concentration as follows: 10 mg/mL in methanol, 15 mg/mL in acetone and 45 mg/mL in DMSO. By controlling addition rate in 1 mL/min, organic solution containing DTG was added into 100 mL of aqueous solution containing 1.0 wt% poloxamer 338, a hydrophilic surfactant. Magnetic stirring was kept in 250 rpm to improve heat and mass transfer on mixing. Experiments were performed at controlled temperature of 25 °C for methanol and DMSO, and from 5 °C to 30 °C in acetone. Acetone was

selected for temperature evaluation due to its rapid evaporation at low temperatures. Solid precipitation occurred immediately upon mixing by a rapid desolvation of DTG in aqueous antisolvent. Suspension was stirred for 60 minutes under 250 rpm to stimulate particle growth. The resulting suspension was sieved through the 53 µm-stainless steel sieves and filtered by 14 µm-paper filter for particle size controlling. Filtered solid was dried overnight under vacuum at 700 mmHg and 60 °C.

Scanning Electron Microscopy (SEM)

Size and the morphology of particles were examined by Field Emission Scanning Electronic Microscopy (Quanta 250 FEG-SEM). Samples were coated with a layer of gold and palladium of 5–10 nm by the cathode dispersion method.

Laser Diffraction

The particle size distribution (PSD) was assessed by laser diffraction particle size analyzer (LS 13320, Beckman Coulter). The instrument employs the polarization intensity differential of scattered light (PIDS) system, which uses polarized beams of 475-, 613-, and 900-nm wavelength and measures particle size over the range of 0.017 to 2000 µm. Samples were dispersed in Tween 80-water solution and slowly added to a suitable compartment of the equipment, containing deionized water (n=1.33 at 20°C), and subjected to a 5-min ultrasonication at energy level 3 to prevent particle agglomeration. Three consecutive runs were performed for each sample. The calculation was performed according to Fraunhofer diffraction model.

Powder X-ray Diffraction (PXRD)

X-ray diffraction patterns of particle powders were studied by using a Phaser X-ray diffractometer (Bruker). Radiations generated from CuKα source and filtered through Ni filters with a wavelength of 0.154 nm (1.541 Å) at 10mA and 30 kV were used to study the X-ray diffraction patterns. The instrument was operated in the continuous mode over the 2θ range of 2-40° with a step size of 0.02°.

Differential Scanning Calorimetry (DSC)

DSC analysis was performed using TA Instrument (Q2000) operating. Temperature axis and cell constant

were calibrated using indium. The samples were exposed to 10 °C /min - heating rates over a temperature range of 25 - 300 °C under nitrogen purging (50 mL/min) in aluminium pans covered by pin-holed lid.

In vitro DTG release testing

Drug release from a modified-release parenteral dosage form is a complex phenomenon and currently, there are no compendial or regulatory guidances because each drug formulation carries its own unique obstacles. As a scenario case-by-case, in in vitro testing of DTG samples, poloxamer 338 was incorporated into the media to prevent DTG particle agglomeration and increase particle wettability. Due to its surfactant properties, Poloxamer 338 has been used in long-acting parenteral formulation development (Baert et al; 2009, vant´Klooster et al; 2010).

Procedure: Twenty-five milligrams of DTG particles (n = 2) were suspended in 2 mL of 2.5% w/v poloxamer-338 aqueous solution and transferred to a dialysis bag membrane (Spectrum Labs, MWCO 12-14kDa). Dialysis bag was suspended in 500 mL phosphate buffered saline (PBS, pH 7.4) and maintained at 37 ± 0.5 °C. The dispersion was rotated at 100 rpm in an orbital shaker. At predetermined time intervals (1h, 2h, 4h, 8h, and from 1st to 20th days), 3-mL aliquots were sampled and DTG concentration was quantified using UV-Vis spectroscopy at 258 nm. After analysis, aliquots were returned to PBS media. The amount of DTG in each sample was calculated based on a calibration curve. Experiments were conducted in duplicate.

In vivo pharmacokinetic study

Ethics: animal procedure was approved by the local ethics committee on animal experiments (CEUA-UNICAMP-protocol number 4666-1/2017, http://www.ib.unicamp.br/comissoes/ceua_principal), complying with Brazil regulation for animal experiments (brazilian federal law number 11794, 2008; CXLV (196): 1-2]) and Guideline for care and use of animals in teaching and in scientific research – (decree number 6899, 2009). **Procedure**: in pharmacokinetic study, male Wistar rats weighting 250-270g (n = 6), with 3 animals for each group, received 5 mg/kg subcutaneous (SC) dose at thoracic region. For injections, DTG was prepared to a 2

mg/mL-DTG particles dispersed in a low viscous aqueous vehicle (0.9% w/v NaCl + 2% w/v Poloxamer 338). Drug concentration was based on toxicokinetics studies of dolutegravir free-base. This study characterized the toxicokinetics of dolutegravir microsuspensions (34-72 μm, D50) following a single subcutaneous (SC) or intramuscular (IM) injection (2.5 mg/kg and 5.0 mg/kg) in male Sprague Dawley rats, (GlaxoSmithKline, 2014). Additionally, in in vivo test, Poloxamer-338 concentration was adjusted to 2.5 % w/v, according to 0.5% w/v of surfactant residue on surface of DTG crystal after LAS process (HPLC data not shown). Blood sampling: at predetermined interval, blood samples (0.25 mL) were withdrawn via puncture from the lateral tail vein. The sampling time point for first group (n=3 rats) was 0, 2h, 4h, 8h, 48h, 96h, 7d, 14d, 21d, 28d, 35d, 42d; whereas for second group (n=3 rats), sampling time was 0, 6h, 12h, 24h, 72h, 7d, 14d, 21d, 28d, 35d, 42d. Blood samples were harvested into heparinized tubes, immediately centrifuged (2000g x 10 minutes) and stored at −70 °C until assay. Sample preparation: plasma samples were processed by following the procedure where 0.25 mL of plasma sample was mixed with Elvitegravir (internal standard) and vortexed for 5 seconds. The mixture was extracted with proper solvent for 5 seconds. After centrifugation for 10 min, organic layer was taken and dried under nitrogen stream at 45 °C. Sample analysis: the dried residue samples were reconstituted using the mobile phase as reconstitution solution. Chromatographic separation was performed on xBridge column (C18 - 5 um) with a isocratic mobile phase composed of acetonitrile and water in the ratio of 80: 20 (v/v) + 0.1% formic acid, at flow-rate of 0.4 mL/min. Dolutegravir and elvitegravir were detected with proton adducts at m/z420.20→277.20 and 448.40→344.20 in multiple reaction monitoring (MRM) positive mode respectively. The method was validated over a linear concentration range of 30–10000 ng/mL for dolutegravir. The lower limit of quantification was 10ng/mL. Analytes were found to be stable throughout freeze-thaw cycles, bench top and postoperative stability studies. This method was successfully applied for the pharmacokinetic analysis of rat plasma samples following subcutaneous administration. Calculation of PK parameters: the mean plasma concentration-time profile was analyzed by non-compartmental analysis (NCA) using Phoenix WinNonlin® v. 7.0 for the pharmacokinetics parameters determination.

RESULTS AND DISCUSSION

The aim of this study was to evaluate the feasibility of a monthly long acting injectable suspension based on DTG. The success of long acting release depends on drug characteristics, such as solid state properties and particle size. Thus, especial emphasis was placed on these properties.

DTG Solubility

Raw DTG solubility was experimentally obtained in methanol, acetone and DMSO and solubility order was found to vary as DMSO > acetone > methanol, Table 1.

Table 1. Raw DTG solubility in methanol, acetone and DMSO

Solvent	Dolutegravir solubility (mg/mL)
Methanol	< 10
Acetone	< 15
DMSO	> 45

According to Table 1, DTG solubility is much higher in DMSO than acetone and methanol. It is accepted that drug solubility depends on its structure and additionally, it can largely be a function of the solvent properties. DTG structure contains two H-donors groups and several H-acceptor groups, (Figure 1), and further, it is a moderately polar compound (Duwal et al; 2018). Relying on the solvent polarity index, polarity can be placed as follows: DMSO (7.2) > acetone (5.1) = methanol (5.1), (Reichardt, 2003). DMSO presents a highly polar domain characterized by a hydrophilic sulfoxide group and two hydrophobic methyl groups (Gurtovenko and Anwar, 2007). Such characteristics provide amphipathic properties to the molecule, making it a good solvent for poorly water soluble DTG.

Anti-solvent crystallization

Anti-solvent crystallization technique produces crystals from solutions and controls the crystalline properties such as particle size and their morphology (Kurup and Arun, 2016). In crystallization process, the antisolvent reduces the solubility of solute in the solution and induces crystallization. Crystallization process is considered a complex kinetic phenomenon that depends on a number of parameters, such as solvent properties and temperature. Further,

nucleation and crystal growth are the main events and govern the final polymorph formation (Datta and Grant, 2005). In this work, DTG precipitation was reached by solution supersaturation when water was added as an antisolvent into organic DTG solution.

X-Ray Diffraction

Temperature and solvent effect on DTG polymorph

X-ray diffraction analyses were performed for DTG particles obtained from DMSO (DTG-DMSO), acetone (DTG-ACE) and methanol (DTG-MeOH), Figure 2. For comparison, raw DTG was also evaluated.
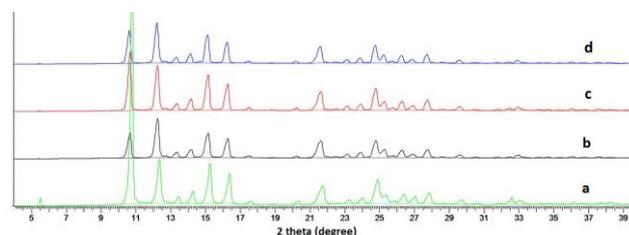
Fig. 2. Powder X-ray diffraction patterns of crystalline DTG. (a) Raw DTG free acid, (b) DTG-DMSO, (c) DTG-ACE and, (d) DTG-MeOH.

Polymorph I of raw DTG free acid is a crystalline structure described by diffraction peaks in 10.753°, 12.324°, 13.437°, 14.251°, 15.234°, 16.352°, 21.697°, 23.996°, 24.867°, 25.341°, 26.373° and, 27.829° at 2θ positions, Figure 2a. To the best of our knowledge, only the polymorphic form I of DTG free acid is known (Yoshida et al; 2014). Therefore, in this work, peaks positions in PXRD patterns were attributed accordingly.

By comparing PXRD for particles obtained from DMSO, acetone, methanol and raw DTG, it is a straightforward observation that polymorph I was particularly maintained after precipitation, although the diffraction peaks are less intense, Figures 2b-2d. The reduction in the peak intensity is due to the decrease in the crystallinity after precipitation (Kayrak *et al*; 2003). Taking into account that solvents acts by selective adsorption to specific crystal faces, either inhibiting or retarding crystal faces growth (Berkovitch-Yellin et al; 1985), we suggest that solvent polarities differences are not enough to specific adsorption.

Particles obtained from acetone (DTG-ACE) under different temperatures were also studied by X-ray diffraction, Figure 3. Similar to particles precipitated

from different solvents, crystallization of DTG in acetone at temperatures of 5°C (DTG-ACE-5°C), 20°C (DTG-ACE-20°C), and 30°C (DTG-ACE-30°C) maintained the polymorphic structure. X-ray diffraction results revealed that, within the experimental conditions, the growth rate of polymorph I of DTG free acid was higher if compared to growth rate of any novel polymorph.

The effect of temperature on the crystallization of DTG from acetone solution was also studied by DSC. It was found that melting peak temperatures and heat of fusion for raw DTG and acetone-precipitated particles are quite similar, Table 2. Thus, as previously observed for solvent, the temperature effect also failed to cause any polymorphic change of DTG.
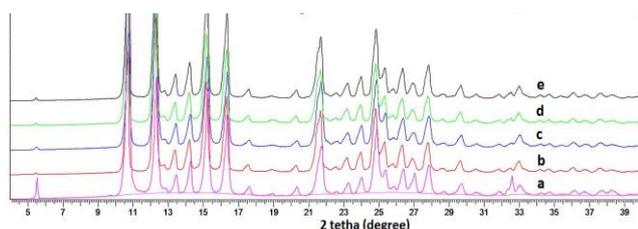
Fig. 3. Powder X-ray diffraction patterns of crystalline dolutegravir precipitated from acetone at different temperatures: (a) raw DTG, (b) DTG-ACE-5°C, (c) DTG-ACE-20°C, (d) DTG-ACE- 25°C and (e) DTG-ACE-30°C.

Differential Scanning Calorimetry

Further, DSC confirmed the identity of polymorphic form I and Figure 4 shows the thermal profiles of raw and crystallized DTG. Both samples showed only an endothermic transition at 191°C due to the melting of polymorph I which occurred with a variation of enthalpy around 80.1 J/g (Yoshida et al; 2014). Therefore, as previously asserted by PXRD, DSC data showed that organic solvent, from which the drug particles crystallized, did not affect the crystal internal structure and polymorphic form was maintained.

Table 2. Thermal values for raw DTG and DTG-acetone particles obtained at different temperatures.

Sample	Tmp (°C)	ΔH (J/g)
Raw DTG	191.33 ± 0.01	78.27 ± 1.6
DTG-ACE- 5°C	191.03 ± 0.02	79.08 ±1.1
DTG-ACE-20°C	190.66 ± 0.02	79.5 ± 1.3
DTG-ACE-25°C	191.08 ± 0.01	79.5 ±1.2
DTG-ACE-30°C	191.27 ± 0.01	83.8 ± 1.4

Tmp: Melting peak temperature, ΔH: Heat of fusion (enthalpy).

Scanning Electron Microscopy

Temperature and solvent effect on DTG crystal morphology

Scanning electron microscopy shows the morphology for raw DTG and particles obtained from DMSO at 25 °C and acetone at 5 °C and 25°C, Figure 5. SEM images showed that raw DTG is composed by micron sized large and compacted agglomerates. Moreover, these structures are assembled by a large number of individual micrometric particles, which exhibit two groups of particle shape, Figure 5a. One group is composed by thick and columnar particles-agglomerates and other one, by quasi-round particles shape. By comparing raw DTG particles (Figure 5a), with DTG-DMSO (Figure 5b) and DTG-ACE-25°C (Figure 5c), solvent effect on particle morphology is undeniable and both precipitated solids exhibited large agglomerates composed of plate-shaped and quasi-hexagonal particles. Clearly there was no difference in particle morphology between DTG-ACE-25°C and DTG-DMSO. Regarding size, DTG-ACE showed agglomerates exceeding 20µm in diameter while DTG-DMSO showed agglomerates not larger than approximately 14µm. Concerning

Fig. 4. DSC thermograms displaying the melting temperature and enthalpy of DTG particles: (a) raw DTG, (b) DTG-DMSO, (c) DTG-ACE and (d) DTG-MeOH.

temperature effect on morphology, it may be noted that as temperature was lowered from 25°C (Figure 5c) to 5°C (Figure 5d), the plate- and quasi-hexagonal shaped micrometric particles organized in large agglomerates of 20μm in diameter. These agglomerates are an assembly of primary particles stick together by adhesion, weak physical interactions (Balakrishnan et al; 2010). In consequence, these larger agglomerates may break down into smaller agglomerates and/or primary particles. In an image-based technique such SEM, a high particle counting is critical to acquiring meaningful information about particle size. Therefore an adequate number of images have to be processed by using appropriate software (Hegela et al; 2014). Although the original morphology of our particles is visible in the agglomerates, they are geometrically assembled in such way that particle size measurement is extremely imprecise, at least in an appreciable number of entities. However, images inspection suggested that DTG-ACE agglomerates are composed of particles around 10μm in size, whereas DMSO-agglomerates are composed of particles less than approximately 2-5μm. In spite of this important difference in particle size, suitable characterization of DTG particle is better given by a particle size distribution once this property impacts directly on drug performance. In this sense, this work explored SEM as a tool for morphology evaluation only. Therefore, as a complementary technique to SEM, laser diffraction was used to measure particle size distribution and polydispersity of DTG particles.
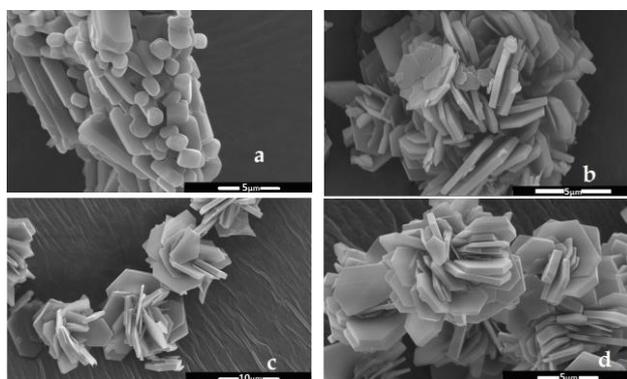
Fig. 5. SEM images of DTG particles: (a) Raw DTG, (b) DTG particles obtained from DMSO at 25 °C (DTG-DMSO), (c) DTG particles obtained from acetone at 25 °C (DTG-ACE-25°C) and (d) DTG particles obtained from acetone at 5 °C (DTG-ACE-5°C). Note different scales.

Laser Diffraction

Solvent effect on DTG particle size

Particle sizes distribution of precipitated and raw DTG was obtained from laser diffraction, Figure 6. DTG-MeOH (Figure 6a) and DTG-ACE (Figure 6b) presented bell-shaped and monomodal curves that describe broad particle size distribution up to 40 μm. Raw DTG showed a bimodal particle size distribution composed of a wide range of particles from very fine to very coarse, Figure 6c. Previously, SEM images also showed that this wide distribution was caused by mixing of multiple particle size and agglomerates, Figure 5a. Particles obtained from DMSO were highly soluble in laser diffraction measurement conditions. We suggested that DTG-DMSO-particles, previously showed in Figure 5b, were loosely agglomerated and they readly disintegrate and dispersed under the measurement conditions (surfactant and ultrasound effects). Therefore, primary small particles caused a positive impact on drug release behavior and anticipated drug solubilization.
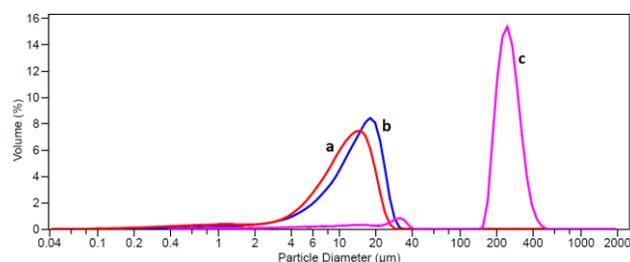
Fig. 6. *Particle size distribution (PSD) volume- weighted for DTG particles obtained from different solvents at room temperature (a) DTG-MeOH, (b) DTG-ACE and (c) raw DTG*

Statistical analysis was performed on particle size distribution curves and the table 3 compares the mean volume-weighted diameter D10, D50, D90. Additionally, the span values which are the measurement of the width of the distribution are provided.

Before processing, raw DTG sample presented large particles in a wide size distribution, as evidenced by span value, Table 3. Clearly the particle size of the precipitated DTG is significantly smaller and more uniform than that of the raw drug. However, as far as solvent is concerned, methanol led to small particle size. Acetone, in its turn, led to narrower particle size distribution, as suggested by span values, Table 3. Naturally, a narrow particle size distribution is preferred as particle size may have a significant

impact on drug release behavior, mainly for compounds that show the drug release rate dependent in vivo exposure as the hydrophobic dolutegravir.

Temperature effect on particle size precipitated from acetone

Figure 7 shows particle size distributions for DTG-ACE at different temperatures. As temperature increased from 5 °C (Figure 7a) to 30 °C (Figure 7d), wider particle size distribution was obtained and size distribution curve assumed a multimodal profile. Statistical analysis results are presented in Table 4.
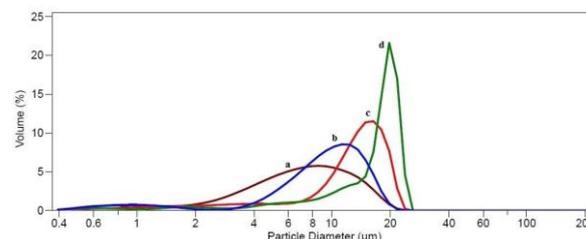
Fig. 7. *Particle size distributions (PSD) volume-weighted for DTG particles obtained from acetone at different temperatures: (a) DTG-ACE-5°C, (b) DTG-ACE-20°C, (c) DTG-ACE-25°C and (d) DTG-ACE-30°C*

Table 3. *Particle size and standard deviation (SD) for DTG particles precipitated from acetone and methanol at 25°C.*

Sample	D10 ± SD (µm)	D50 ± SD (µm)	D90 ± SD (µm)	Span[a]
Raw DTG	36.9 ± 3	240 ± 3	327 ± 4	1.21
DTG-ACE	3.15 ± 0.08	13.4 ± 0.09	19.1 ± 0.49	1.19
DTG-MeOH	2.89 ± 0.16	10.6 ± 0.40	18.0 ± 0.55	1.42

[a] The span is the measurement of the width of the particle size distribution defined as (D90 – D10)/D50.

Table 4. *Particle size and standard deviation (SD) for DTG particles precipitated from acetone at different temperatures.*

Sample	D10 ± SD (µm)	D50 ± SD (µm)	D90 ± SD (µm)	Span[a]
DTG-ACE-5 °C	2.60 ± 0.65	9.27 ± 0.75	13.7 ± 1.13	1.19
DTG-ACE-20 °C	1.76 ± 0.26	6.48 ± 0.41	12.5 ± 1.65	1.65
DTG-ACE-25 °C	3.15 ±0.08	13.4 ± 0.09	19.1 ± 0.49	1.18
DTG-ACE-30 °C	4.16 ± 0.94	17.2 ± 0.69	20.7 ± 1.07	0.95

[a] The span is the measurement of the width of the particle size distribution defined as (D90 – D10)/D50

The temperature is considered as an important governing factor which can control the final particle size and its distribution. Table 4 shows that when crystallization occurred at 5 °C or 20 °C, smaller particles were produced for DTG. Although temperature had no greater effect on particle size in this temperature range, the smallest particle size occurred at 20 °C. Remarkably, as the temperature increased from 20 °C to 25 °C, particle size increased twofold. Further, particle size increased 23 % when the temperature increased to 30 °C. Span values indicated the particle size distribution width is quite close among samples, but the wider particle size distribution occurred when DTG precipitated at 20°C. It is important to keep in mind that the theory of crystallization suggests that the rate of nucleation is inversely proportional to temperature (Fujiwara *et al*; 2005). At low temperature, the solubility of the drug in the solvent-antisolvent mixture decreases, which results in the higher supersaturation condition (Kurup and Arun; 2016, Judge *et al*;1999). In a cascade

effect, supersaturation drives a competition between nucleation and crystal growth rates (Liang and Zang, 2017). Accordingly, as low temperature decreases the diffusion and growth kinetics at the crystal boundary layer interface, nucleation rate can increase and lead to a large number of nuclei and this stage accelerate precipitation event. As a result, smaller drug particles are obtained at low temperature.

In vitro drug release profiles

Figure 8 shows *in vitro* drug release profiles for raw DTG and DTG precipitated from acetone. **As shown in Figure 8, in comparison with raw DTG, clearly the particle size of DTG-ACE samples affected *in vitro* DTG release profile. In fact, at the 12th day of testing time, samples DTG-ACE-5°C and DTG-ACE-20°C, containing small-sized particles, Table 4, showed a maximum drug release of 92%. Whereas samples DTG-ACE-25°C and DTG-ACE-30°C showed a maximum drug release of 88%. Because of**

the larger particle size, raw drug showed a maximum release of only 47.5% in the same period.
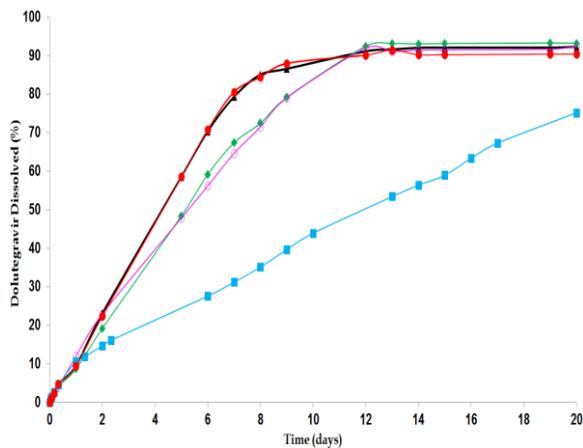
Fig. 8. *In vitro release profile of DTG particles:* ■ *raw DTG (240 μm),* ● *DTG-ACE-5°C (9.27 μm),* ▲*DTG-ACE-20°C (6.48 μm),* ○ *DTG-ACE-25°C (13.4 μm) and* ◆*DTG-ACE-30°C (17.2 μm). Note particle size value (D50) after sample code.*

On the other hand, by comparing these samples amongst themselves, they presented similar *in vitro* release behaviors once particles size is quite close. According to Noyes-Whitney equation (Noyes and Whitney, 1985), one should assume proportionality between the rate of drug release and particle surface area. Therefore, decreasing particle size (i.e increasing the surface area) should increase the contact between particle surfaces and medium. Consequently, drug release rates are lower with larger particles. This statement suggests that particle size reduction and particle size distribution affected the drug release rate of DTG. Additionally, DTG-ACE samples showed higher drug release rates because these particles have lower crystallinity and more uniform morphology than raw DTG, as previously indicated by XRD and SEM, respectively. Crystal defects and imperfections influence the crystal lattice energy. These defects, including dislocations, give rise to increased surface energy and may be an important factor in improving drug release performance of DTG-ACE particles. Moreover, particle morphology dictates the drug release rate along the different crystallographic axes (Bukover et al; 2015). So altering shape of DTG particles from round (raw DTG) to plate-like shape (DG-ACE) may lead to higher drug release rate. The enhanced drug

release rate of DTG-ACE particles is due to the reduction of the particle size, change in crystaline habit, and reduction in crystallinity of DTG during precipitation, formation of hydrophilic surface and the increased wettability caused by adsorption of poloxamer-338. The results of in vitro drug release testing indicated that DTG-ACE particle properties allow DTG release sustaining for 12 days. Naturally, DTG-ACE particles are intended to modified-release dosage form whose drug release rate is the performance-limiting step. Besides, as a direct implication on a future DTG-long acting injectable formulation, it may be previewed that higher the drug release rate together with the resulting higher concentration gradient could further increase drug bioavailability. On the other hand, in early stage, *in vitro* and *in vivo* correlation may not be possible due to the complexity of the release mechanism, and the lack of knowledge about *in vivo* release conditions. Therefore, *in vitro* drug release testing worked as a promising tool for effective DTG microparticles characterization only.

Pharmacokinetic profiles for DTG particles

To gain further insight on effect of particle size reduction on DTG pharmacokinetics, an exploratory study evaluated the *in vivo* behavior of DTG-ACE-25°C sample, **Table 4**. Figure 9a shows the mean plasma concentration-time profile of DTG obtained after subcutaneous administration of 5 mg/kg in male rats during 42 days. Figure b displays the mean plasma concentration-time profile of DTG for first 90 hours. Additionally, Figures 9a and 9b show a line to indicate PA-IC90 (64ng/mL). Table 5 displays the Mean pharmacokinetic parameters, for DTG, obtained by non-compartmental analysis.

Exploring the concentration time profile, Figure 9a, it can be found that plasma DTG concentrations increased rapidly, resulting in a double-peak that was followed by a slow decline of drug concentrations. DTG was detected in plasma from the first blood sampling time (2h) and C_{max} value of 645 ng/mL at the time point of 12h (tmax) were measured, (Figure 9a and Table 5). Although plasma concentrations have gradually declined, they were maintained above PA-IC90 (64 ng/mL) for 26 days after administration. DTG plasma concentrations were measurable until 35 days and, in the last

sampling time, (42 days), it was below the lower limit of quantification, (10 ng/mL).

Making an assumption that only drug release rate limits DTG plasma concentrations, the results are a straight reflection from different fine particle fractions provided by liquid antisolvent precipitation. Our hypothesis is that the smallest particle size, with their large surface area, readily resulted in burst release and in an expressive drug concentration 10-fold higher than PA-IC90 in the first 90 hours. Larger particle size, in turn, should be responsible for second and more prolonged pharmacokinetic exposure. Based on current findings, it is possible to deduce that a more rigorous and narrower particle size distribution is mandatory.
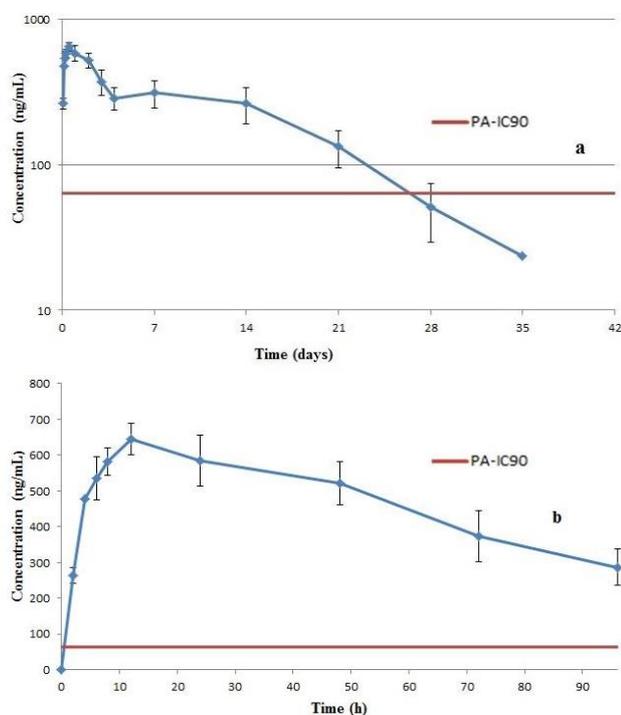
Fig. 9. Mean plasma concentration-time profiles of DTG after subcutaneous administration of DTG 5 mg/kg (dispersed in 2% poloxamer 338 + 0.9% NaCl) in rats (n = 6): a) 35 days-profile and b) First four days profile. Vertical bars represent standard deviation. Particle size description: D10 = 3.15 µm, D50 = 13.4 µm and D90 = 19.1 µm.

In fact, Silman *et al,* (2018), showed that 368nm-DTG particles maintained plasma drug concentrations above the PA-IC90 for 14 days in mice treated with a dose of 45 mg/kg. Further, our current result showed that particle size larger than 13µm sustains *in vivo* DTG concentration above PA-IC90 for 26 days. However, microparticles-based injectable suspensions are extremely challenging because they

are systems prone to physical instability such as caking, sedimentation and particle growth. Ultimately, larger particles increase the viscosity of suspensions, hindering syringeability as well as injectability and further promote syringe clogging.

Table 5. Mean pharmacokinetic parameters determined by non-compartmental analysis following 5 mg/kg SC dosing in Wistar rats.

Pharmacokinetic parameters	Mean (DTG-ACE-25 °C)
tmax (h)	12.0
Cmax (ng/mL)	645.0
$t_{1/2}$ (h)	141.7
AUC 0-t (h*ng/mL)	169,823.2
AUC 0-inf (h*ng/mL)	174,611.3
tc > PA-IC90 (day)	26.0

t_{max}: time to reach maximum (peak) plasma concentration following drug administration; C_{max}: maximum (peak) plasma drug concentration, $t_{1/2}$: half-life time, **AUC** $_{0-t}$: area under the plasma drug concentration-time curve from time zero to the last quantifiable time (35 days), **AUC-** $_{0-inf}$: Area under the plasma concentration-time curve from time zero to infinity. t_c : time interval during which plasma drug concentrations are above PA-IC90.

CONCLUSIONS

The aim of this study was to engineer a proper particle size to provide plasma dolutegravir concentration maintenance above protein-adjusted 90% inhibitory concentration (PA-IC90) and to evaluate the monthly-acting injectable dolutegravir feasibility. Concerning drug exposure, our sample DTG-ACE-25°C showed satisfactory results and plasma drug concentration was above PA-IC90 for 26 days. However, microparticle-based injectables pose hard-manageable issues such as worsen syringeability, suspension stability and larger injection volumes as well. Although all potential of DTG microparticle-based suspensions as a future perspective for DTG long-acting has not been thoroughly investigated, the obtained results suggested that different approaches to adequately address the challenges in development of such product are strongly recommended.

REFERENCES

Baert, L., van't Klooster, G., Dries, W., Francois, M., Wouters, A., Basstanie, E., Iterbeke, K., Stappers, F.,

Stevens, P., Schueller, L., Van Remoortere, P., Kraus, G., Wigerinck, P., Rosier, J., 2009. Development of a long-acting injectable formulation with nanoparticles of rilpivirine (TMC278) for HIV treatment. Eur. J. Pharm. and Biopharm., 72, 502-508.

Balakrishnan, A., Pizette, P., Martin, C. L., Joshi, S. V., Saha, B. P., 2010. Effect of particle size in aggregated and agglomerated ceramic powders. Acta Mater., 58, 802–812.

Benzon, H. T., Chew, T-L., McCarthy, R. J., Benzon, H. A., Walega, D. R., 2007. Comparison of the particles sizes of different steroids and the effect of dilution. Anesthesiology, 106, 331-338.

Berkovitch-Yellin, Z., van Mil, J., Addadi, L., Idelson, M., Lahav, M., Leiserowitz, L., 1985. Crystal morphology engineering by "tailor-made" inhibitors; a new probe to fine intermolecular interactions. J. Am. Chem. Soc., 107, 3111-3122.

Bukover, P., Meden, A., Smrkolj, M., Vrecĕr, F., 2015, Influence of crystal habit on the dissolution odf simvastatin single particles. Acta Chim. Slov; 62, 958-966.

Cottrell, M. L., Hadzic, T., Kashuba, A. D., 2013. Clinical pharmacokinetic, pharmacodynamic and drug-interaction profile of the integrase inhibitor dolutegravir. Clin. Pharmacokinet. 52, 981-984.

Datta, S., Grant, D. J. W., 2005. Effect of supersaturation on the crystallization of phenylbutazone polymorphs. Cryst.Res. Technol., 40(3), 233-242.

Duwal, S., Dickinson, L., Khoo, S., von Kleist, M., 2018. Hybrid stochastic framework predicts efficacy of prophylaxis against HIV: An exemple with different dolutegravir prophylaxis shemes. PLoS Comput. Biol. 14(6): e1006155. doi.org/10.1371/journal.pcbi.1006155.

Fujiwara, M., Nagy, Z. K., Chew, J. W., Braats, R. D., 2005. First-principles and direct design approaches for the control of pharmaceutical crystallization. J. Process. Control., 15(5), 493-504.

GlaxoSmithKline, 2014. Module 2.6.4. Pharmacokinetics Written Summary (2012N154235_00). http://www.pmda.go.jp/drugs/2014/P2014000 46/340278000_22600AMX00561_I100_1.pdf. Extracted form google.

Gurtovenko, A. A., Anwar, J., 2007. Modulating the structure and properties of cell membranes: The molecular mechanism of action of dimethyl sulfoxide J. Phys. Chem. B., 111, 10453-10460.

Hee-Jeong, K., Sang-Do, Y., 2015. Liquid antisolvent crystallization of griseofulvin from organic solutions. Chem. Eng. Res. Des., 97, 68-76.

Hegela, C., Jones, C., Cabrera, F., Yáñezb, M. J., Bucala V., 2014, Particle size characterization comparison of laser diffraction (LD) and scanning electron microscopy (SEM). Acta Micros., 23(1), 11-17.

Jones, D. S., 2016. Pharmaceutics-Dosage Form and Design. London : Pharmaceutical Press, 2nd edition, 138

Judge, R. A., Jacobs, R. S., Frazier, T., Snell, E. H., Marc L. Pusey, M. L., 1999. The effect of temperature and solution pH on the nucleation of tetragonal lysozyme particles. Biophys. J., 77, 1585–1593.

Kayrak, D., Akman, U., Hortacsu, O., 2003. Micronization of ibuprofen by RESS. J. Supercrit. Fluids, 26(1), 17-31.

Kurup, M., Arun, R. R., 2016. Antisolvent crystallization: A novel approach to bioavailability enhancement. European J. Biomed. Pharm. sci., 3 (1-2), 230-234.

Liang, Z., Zhanga, M., Wua, F., Chena, J-F., Xuec, C., Zhao, H., 2017. Supersaturation controlled morphology and aspect ratio changes of benzoic acid crystal. Comput. Chem. Eng., 99, 296-303.

Lonare, A. A., Patel, S. R., 2013. Antisolvent crystallization of poorly water soluble drugs. Int. J. Chem. Eng. Appl., 4(5), 337-341.

Meer, T. A., Sawant, K. P., Amin, P. D., 2011. Liquid antisolvent precipitation process for solubility modulation of bicalutamide. Acta Pharm., 61, 435-445.

Noyes, A. A., Whitney, W. R., 1987. The rate of solution of solid substancens in their own solutions. J. Am. Chem. Soc., 19:930-934.

Osterholzer, D. A., Goldman, M., 2014. Dolutegravir: A next-generation integrase inhibitor for treatment of HIV infection. Clin. Infect. Dis., 59, 265-271.

Owen, A., Rannard, S., 2016. Strengths, weaknesses, opportunities and challenges for long acting injectable therapies: insights for applications in HIV therapy. Adv. Drug Deliv. Rev., 1,144-156.

Rajoli, R. K. R., Back, D. J., Rannard, S., Meyers, C. F., Flexner, C., Owen, A., Siccard, M., 2015. Physiologically-based pharmacokinetic modelling to inform development of intramuscular long-acting nanoformulations for HIV. Clin. Pharmacokinet., 54(6), 639-650. doi:10.1007/s40262-014-0227-1.

Reichardt, C., 2003. Solvents and Solvents Effects in Organic Chemistry. Weinheim : Wiley-VCH, 3rd.

Sillman, B., Bade, A. N., Dash, P. K., Bhargavan, B., Kocher, T., Mathews, S., Su, H., Kanmogne, G. D., Poluektova, L. Y., Gorantla, S., McMillan, J., Gautam, N., Alnouti, Y., Edagwa, B., Gendelman, H. E., 2018. Creation of a long-acting nanoformulated dolutegravir. Nature Comm., 9. DOI: 10.1038/s41467-018-02885-x.

Swindells, S., Andrade-Villanueva, J-F., Richmond, G. J., Rizzardini, G., Baumgarten, A., Masia, M. D. M.., Latiff, G., Pokrovsky, V., Mrus, J. M., Huang, J. O., Hudson, K. J., Margolis, D. A., Smith, K., Williams, P. E., Spreen W., Long-acting cabotegravir + Rilpivirine as maintenancne therapy : ATLAS week 48 results. http://www.croiwebcasts.org/p/2019croi/139

Thorat, A. A., Dalvi, S. V., 2012. Liquid antisolvent precipitation and stabilization of nanoparticles of poorly water-soluble drugs in aqueous suspensions: Recent developments and future perspective. Chem. Eng. J., 181-182, 1-34.

Trezza, C., Ford, S. L., Spreen, W., Pan, R., Piscitelli, S., 2015. Formulation and pharmacology of long-acting cabotegravir. Curr. Opin. HIV AIDS, 10, 239-245. DOI:10.1097/COH.0000000000000168.

van´t Klooster, G., Hoeben, E., Borghys, H., Looszova, A., Bouche M-P., van Velsen, F., Baert, L., 2010. Pharmacokinetics and disposition of rilpivirine (TMC278) nanosuspension as a long-acting injectable antiretroviral formulation. Antimicrob. Agents Chemother., 54, 2042-2050. doi:10.1128/AAC.01529-09.

Yoshida, H., Taoda, Y., Johns, A., Kawasuji, T., Nagamatsu, D., Inventors. Shionogi & Co., Ltd, ViiV Healthcare Company, Assignees. Synthesis of carbamoylpyridone HIV integrase inhibitors and intermediates: United States Patent US 0243,521 A1. United States, 28 de august de 2014.